ACS APPLIED MATERIALS & INTERFACES

www.acsami.org Research Article

Gold Nanorod Size-Dependent Fluorescence Enhancement for Ultrasensitive Fluoroimmunoassays

Chao Liang,○ Jingyi Luan,○ Zheyu Wang, Qisheng Jiang, Rohit Gupta, Sisi Cao, Keng-Ku Liu, Jeremiah J. Morrissey, Evan D. Kharasch, Rajesh R. Naik,* and Srikanth Singamaneni*

Cite This: *ACS Appl. Mater. Interfaces* 2021, 13, 11414−11423 Read Online

ABSTRACT: Plasmon-enhanced fluorescence (PEF) is a simple and highly effective approach for improving the signal-to-noise ratio and sensitivity of various fluorescence-based bioanalytical techniques. Here, we show that the fluorescence enhancement efficacy of gold nanorods (AuNRs), which are widely employed for PEF, is highly dependent on their absolute dimensions (i.e., length and diameter). Notably, an increase in the dimensions (length × diameter) of the AuNRs from 46 × 14 to 120 × 38 nm^2 while holding the aspect ratio constant leads to nearly 300% improvement in fluorescence enhancement efficiency. Further increase in the AuNR size leads to a decrease of the fluorescence enhancement efficiency. Through finite-difference time-domain (FDTD) simulation, we reveal that the size-dependent fluorescence enhancement efficiency of AuNR stems from the size-dependent electromagnetic field around the plasmonic nanostructures. AuNRs with optimal dimensions resulted in a nearly 120-fold enhancement in the ensemble fluorescence emission from molecular fluorophores bound to the surface. These plasmonic nanostructures with optimal dimensions also resulted in a nearly 30-fold improvement in the limit of detection of human interleukin-6 (IL-6) compared to AuNRs with smaller size, which are routinely employed in PEF.

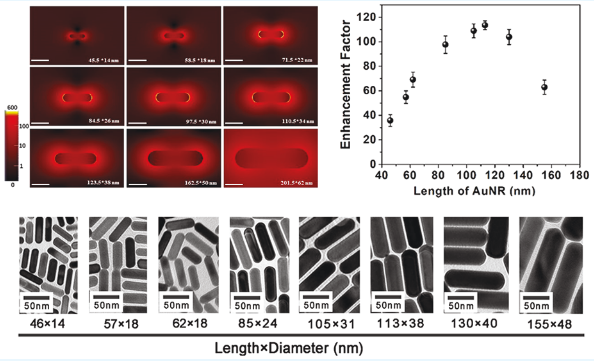

KEYWORDS: *plasmon-enhanced fluorescence, gold nanorod (AuNR), plasmonic patch, fluoroimmunoassay, protein microarray*

■ INTRODUCTION

Fluorescence-based sensing and imaging methods are widely employed in biomedical research and clinical diagnostics. However, these methods generally suffer from poor sensitivity due to the feeble fluorescence signal of conventional molecular fluorophores, resulting in low signal-to-noise ratio. It is known that fluorescence emission from organic dyes and inorganic emitters can be significantly enhanced by the intense electromagnetic field around plasmonic nanostructures, known as plasmon-enhanced fluorescence (PEF).[1−3] Enhancement in the emission of fluorophores in close proximity to plasmonic nanostructures is attributed to the enhanced electromagnetic field (local excitation field) at the surface of the plasmonic nanostructures and the decrease in the fluorescence lifetime due to the coupling between the excited fluorophores and the surface plasmons of the nanostructures.[4−14] To achieve high fluorescence enhancement efficiency, it is important to design and realize plasmonic nanostructures that exhibit high electromagnetic field enhancement at the surface. For example, coupled plasmonic nanoantennas such as bowtie nanoantennas fabricated by electron-beam lithography resulted in a more than 1000-fold enhancement in fluorescence from single molecules.[6] Several other complex plasmonic nanoconstructs such as antenna-in-box, plasmonic patch antenna,[15] and periodic gold arrays[16,17] also offer a large fluorescence enhancement owing to the intense electromagnetic field generated by plasmonic coupling. However, due to their complex design, these coupled plasmonic nanoconstructs are generally difficult to realize in a controllable and scalable manner.

In contrast, individual nanostructures, especially gold nanorods (AuNRs), are attractive candidates for PEF applications due to their simple and scalable synthesis procedures with well-controlled size and shape, long-term stability, as well as tunable localized surface plasmon resonance (LSPR) wavelength.[18,19] However, commonly employed AuNRs (with a diameter of 10−20 nm and a length of 30−60 nm) exhibit a relatively weak electromagnetic field compared to coupled nanostructures, therefore compromising their fluorescence enhancement efficacy. Here, we demonstrate that the fluorescence enhancement efficiency of AuNR can be

Received: November 13, 2020
Accepted: February 8, 2021
Published: February 23, 2021

https://dx.doi.org/10.1021/acsami.0c20303

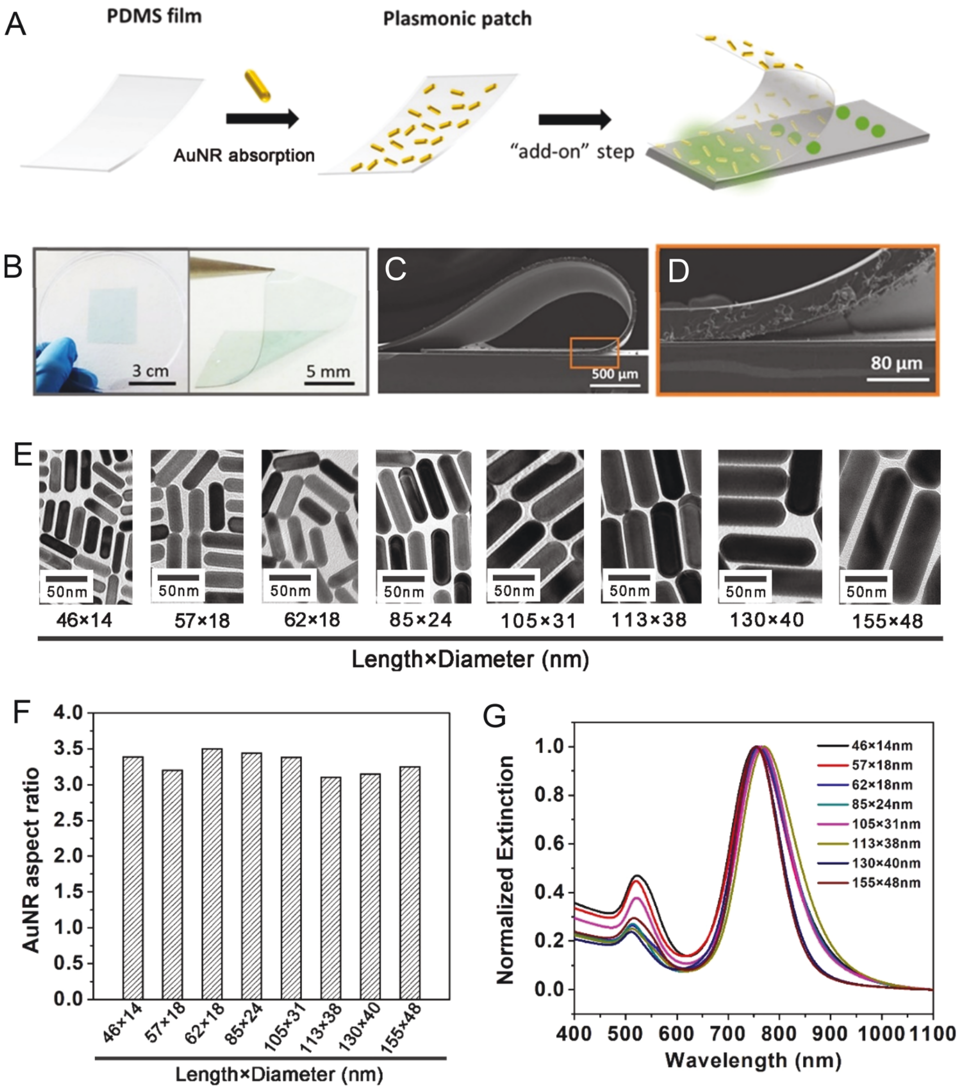

Figure 1. Size-dependent plasmon-enhanced fluorescence using a plasmonic patch. (A) Schematic representation of the simple "add-on" process to enhance the fluorescence emission based on an elastomeric plasmonic patch. (B) Photographs of a plasmonic patch comprised of gold nanorods (AuNRs). (C) SEM image of the plasmonic patch showing the high flexibility. (D) Zoom-in SEM image of the interface between the plasmonic patch and the silicon substrate showing the high conformability. (E) TEM images of AuNRs with increasing size (length × diameter). (F) Aspect ratio of the AuNRs shown in part E. (G) Normalized extinction spectra of the aqueous solutions of AuNRs, showing similar LSPR wavelength.

significantly improved (by up to 300%) by simply optimizing their dimensions (length and diameter). We found that the fluorescence enhancement efficiency increases dramatically with an increase in the size of the AuNRs up to an optimal dimension, followed by a decrease with a further increase in size. AuNRs with optimal dimensions of around 130 nm in length and 40 nm in diameter resulted in a nearly 120-fold enhancement in the fluorescence intensity of a near-infrared dye (800CW) placed in the vicinity of the AuNR.

In this study, we have employed a "plasmonic patch", a thin elastomeric film adsorbed with AuNRs, as the material platform for determining the effect of the dimensions of AuNRs on the fluorescence enhancement. We demonstrate that a "plasmonic patch" comprised of AuNRs with optimal dimensions can be applied to various fluoroimmunoassays as an add-on step to improve their sensitivity without any modifications to the current procedures.[20] Compared to AuNRs with small dimensions, which resulted in a nearly 30-fold improvement, size-optimized AuNRs resulted in a nearly 100-fold improvement in the sensitivity of human interleukin-6 (IL-6) fluoroimmunoassay. Finally, we demonstrate the real-world application of the size-optimized AuNR plasmonic patch for simultaneously enhancing the sensitivity of a 10-plex human cytokine microarray.

■ RESULTS AND DISCUSSION

The plasmonic patch is comprised of a thin polydimethylsiloxane (PDMS) film (thickness of ∼40 μm) with AuNRs uniformly absorbed on the surface. The elastomeric nature of PDMS ensures the conformal contact of the AuNR (on the patch) with fluorescent species on the surface of interest (e.g., fluoroimmunoassay surfaces) (Figure 1A) to effectively enhance the emission of the fluorophores on the surface (Figure 1B−D). Prior to the systematic investigation of the effect of the size of AuNRs on the fluorescence enhancement efficiency, it is important to minimize the potential interference arising from other contributing factors. It is known that an optimal distance between a fluorophore and the metal surface

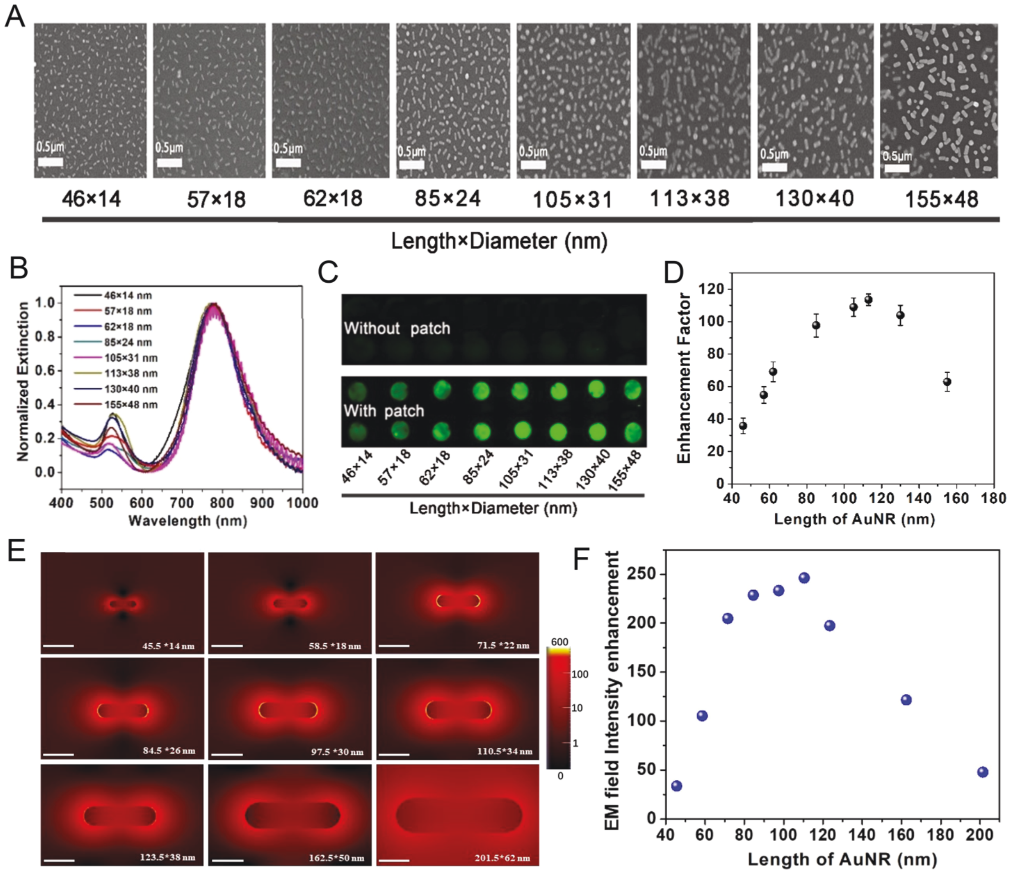

Figure 2. (A) SEM images of the plasmonic patch revealing a similar density of AuNRs on PDMS (size of the AuNRs from left to right: AuNR-46 × 14 nm^2, AuNR-57 × 18 nm^2, AuNR-62 × 18 nm^2, AuNR-85 × 24 nm^2, AuNR-105 × 31 nm^2, AuNR-113 × 38 nm^2, AuNR-130 × 40 nm^2, and AuNR-155 × 48 nm). (B) Vis-NIR extinction spectra of the plasmonic patches comprised of AuNRs with different dimensions after being transferred to a 96-well plate, which exhibit a slight red shift compared to the LSPR wavelength in aqueous solutions. (C) The fluorescence map and (D) calculated enhancement factors of emission of 800CW using the plasmonic patches with AuNRs of different sizes. (E) Finite-difference time-domain (FDTD) simulation, showing the electromagnetic field around AuNRs with different sizes (the scale bar represents 50 nm). (F) Plot showing the electromagnetic field intensity enhancement for AuNRs of different dimensions (from length 46 to 200 nm).

is critical to balance the two opposing effects, namely, metal-induced fluorescence quenching and plasmon enhancement, to realize high fluorescence enhancement efficiency. Based on our previous work, the spacer layer thickness was maintained to be 3 nm across all of the plasmonic patches with various AuNRs.[21] Previous studies have also shown the importance of matching the AuNR LSPR wavelength with the absorbance/emission of the fluorophore to maximize the fluorescence enhancement efficiency.[19,22] We first set out to determine the optimal LSPR wavelength of AuNRs for near-infrared dye, 800CW, which is employed as the model fluorophore in this study.

To investigate the effect of the LSPR wavelength on the fluorescence enhancement, we fabricated plasmonic patches using eight distinct AuNRs with a longitudinal LSPR wavelength ranging from ~700 to 800 nm by increasing their aspect ratio while fixing the diameter. The AuNR density of various plasmonic patches was adjusted to a similar level (92 ± 5/μm^2), as depicted in the SEM images (Figure S1Aa–h). To form a dielectric spacer layer on the AuNRs, two silane monomers, namely, (3-aminopropyl)trimethoxysilane (APTMS) and trimethoxy(propyl)silane (TMPS), were copolymerized on the surface of the AuNRs. As mentioned above, the optimal thickness of the spacer layer was found to be ~3 nm based on our previous study.[20] To test the fluorescence enhancement efficacy, plasmonic patches modified with various AuNRs were transferred onto the bottom of polystyrene wells (of a standard 96-well plate), uniformly coated with 800CW. The LSPR wavelength of the plasmonic patch after its transfer to the 96-well plate surface showed a gradual red shift due to the increase in the effective refractive index of the medium surrounding the AuNRs (Figure S1B). The highest fluorescence enhancement (nearly 45-fold) was obtained for patches comprised of AuNRs with a LSPR wavelength around 758 and 774 nm (Figure S1C and D) (the enhancement factor is defined as the ratio of fluorescence signal intensity after adding the plasmonic patch to the pristine signal). After the transfer to the 800CW coated polystyrene wells, the LSPR wavelength of the plasmonic patches was comprised of AuNR-758 and AuNR-774 shift to 780 and 798 nm, respectively (Figure S1E). The LSPR shift causes a large overlap between the plasmon extinction band of the patches and the absorption/emission bands of the 800CW (Figure 2E). In determining the optimal LSPR wavelength of the nanostructures for fluorescence enhancement using a plasmonic patch, one needs to account for the LSPR shift upon the transfer of the plasmonic patch to the desired surface, which resulted in their high fluorescence enhancement efficiency compared to other nanostructures. Therefore, AuNRs with a

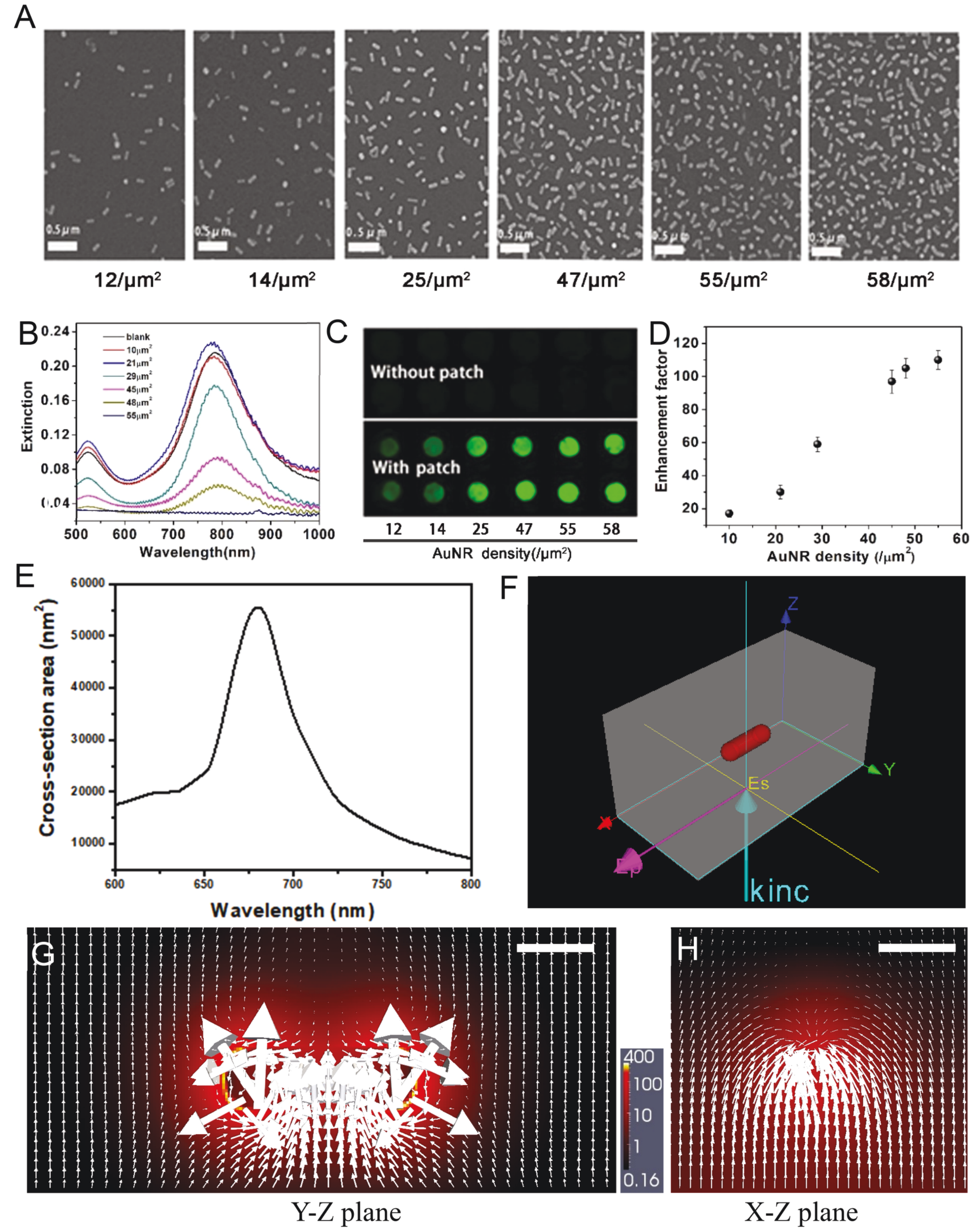

Figure 3. (A) SEM images of the plasmonic patch AuNR-130 × 40 nm^2 with increasing density of AuNRs. (B) Extinction spectra of plasmonic patches of AuNR-130 × 40 nm^2 with different AuNR densities after transferring them to a 96-well plate. (C) Fluorescence maps and (D) plot showing the fluorescence enhancement efficacy of plasmonic patches with different AuNR densities. (E) Simulated spectra (cross-section area) of AuNR-130 × 40 nm^2 with incident light polarized along the long-axis of the AuNR. (F) Illustration showing the finite-difference time-domain (FDTD) simulation of AuNR 130 × 40 nm^2. (G, H) Distribution of the electric field intensity (background) and Poynting vector (white arrows) in the *Y*−*Z* plane and *X*−*Z* plane (scale bars represent 50 nm).

LSPR wavelength around 760 nm were employed in subsequent studies.

Next, we set out to investigate the size effect of the AuNRs on the fluorescence enhancement efficiency. We synthesized AuNRs of different dimensions with a LSPR wavelength of 760 ± 5 nm (Figure 1E and G). As synthesized AuNR exhibited a similar aspect ratio (length/diameter) of around 3.2 (Figure 1F). The AuNR density on each plasmonic patch was fixed to 50 ± 6/μm^2, as evidenced by SEM images (Figure 2A). To form a dielectric spacer layer of similar thickness on the

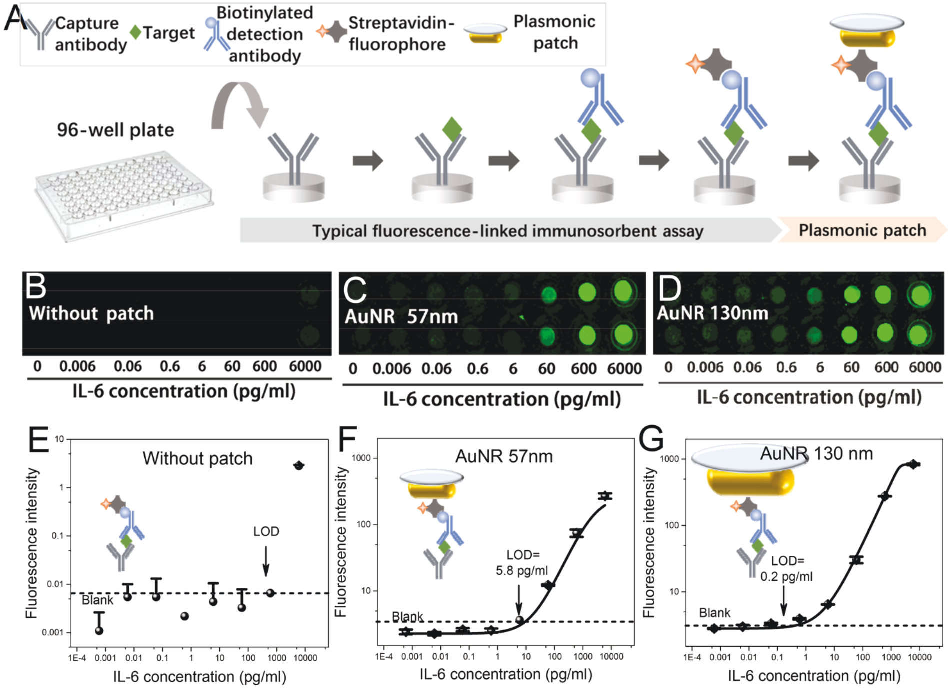

Figure 4. (A) Schematic showing the steps involved in plasmonic-patch-enhanced IL-6 fluoroimmunoassay implemented on a 96-well plate. Fluorescence map of (B) unenhanced IL-6 fluoroimmunoassay, (C) AuNR-57 nm (57 × 18 nm^2) enhanced fluoroimmunoassay, and (D) AuNR-130 nm (130 × 40 nm^2) enhanced IL-6 fluoroimmunoassay. Plot showing the IL-6 dose−response curve of (E) conventional IL-6 fluoroimmunoassay, (F) AuNR-57 nm (57 × 18 nm^2) enhanced fluoroimmunoassay, and (G) AuNR-130 nm (130 × 40 nm^2) enhanced IL-6 fluoroimmunoassay. The size-optimized AuNR leads to an improvement of 3 orders of magnitude in the sensitivity compared to the unenhanced fluoroimmunoassay and a 30-fold improvement compared to the AuNR-57 nm enhanced fluoroimmunoassay.

AuNRs, the same amounts of APTMS and TMPS were copolymerized on the surface of the AuNRs. Plasmonic patches were then transferred onto the bottom of a standard 96-well plate coated with 800CW. After adding the plasmonic patches onto the bottom of the polystyrene wells, the LSPR wavelength exhibited a large overlap with the absorption/emission of 800CW (Figure 2B and Figure S1E). The fluorescence enhancement factor increased rapidly with an increase in the AuNR dimensions (both length and diameter) and reached a maximum for AuNRs with a length of 110 nm (Figure 2C and D). A nearly 120-fold fluorescence enhancement was observed for patches comprised of AuNR-113 × 38 nm^2 (Figure 2C and D) compared to ∼40-fold using AuNRs with smaller dimensions (46 × 14 nm^2). A further increase in the length resulted in a decrease in the fluorescence enhancement factor. The intensity of plasmonic-patch-enhanced fluorescence was found to be 145-fold higher than the autofluorescence of the AuNRs (Figure S3). The low autofluorescence of AuNRs will have a minimal effect on the overall fluorescence signal and the fluorescence enhancement efficiency.

To understand the size-dependent enhancement phenomenon, we performed finite-difference time-domain (FDTD) simulations that revealed the electromagnetic field intensity around AuNRs of different sizes (Figure 2E). The boundary condition (simulation box size) and the mesh size (the grid size) were set to be 400 × 200 × 200 nm^3 and 1 nm, respectively. The electromagnetic field intensity at 3 nm (accounting for the polymer spacer layer) from their surface was found to rapidly increase with an increase in the size of the AuNRs and reached the maximum value for AuNRs with a length of 110 nm. Further increase in the dimensions of the AuNRs resulted in a decrease in the electromagnetic field intensity (Figure 2F). The AuNR size-dependent electromagnetic field intensity deduced from the FDTD simulations showed excellent agreement with the experimentally observed size-dependent fluorescence enhancement. In general, a linear relationship between the EM field enhancement efficiency and the fluorescence enhancement was observed (Figure S2). It is known that, for smaller AuNRs, electron-surface scattering dominates the plasmon damping, while radiation damping rapidly increases with the volume of the AuNRs and becomes the dominant factor for larger nanorods.[23,24] As the size of the AuNR increases, the lightening rod effect, which results in a strong electromagnetic field enhancement at the AuNR end-caps, becomes weaker due to the decrease in the local curvature.[25] Collectively, these factors determine the optimal dimensions of AuNRs for attaining the maximal field enhancement at the surface of the AuNRs.

Next, we evaluated the effect of the density of these plasmonic nanostructures (on PDMS film) on the fluorescence enhancement efficiency. We have fabricated plasmonic patches with different densities of AuNRs with a length of 130 nm and a diameter of 40 nm by increasing the concentration of the AuNR solution deposited on the PDMS film (Figure S4). SEM images depict plasmonic patches with a AuNR density of 12.0 ± 2.6/μm^2, 14.2 ± 3.1/μm^2, 25.3 ± 2.2/μm^2, 47.3 ± 2.8/μm^2, 55.4 ± 2.8/μm^2, and 57.8 ± 3.7/μm^2 (Figure 3A). Correspondingly, the plasmonic extinction intensity of the patches showed a gradual increase with an increase in the density of AuNRs (Figure 3B). These plasmonic patches were transferred onto the bottom of a standard 96-well plate coated with 800CW. We observed a density-dependent fluorescence enhancement (Figure 3C). The fluorescence enhancement

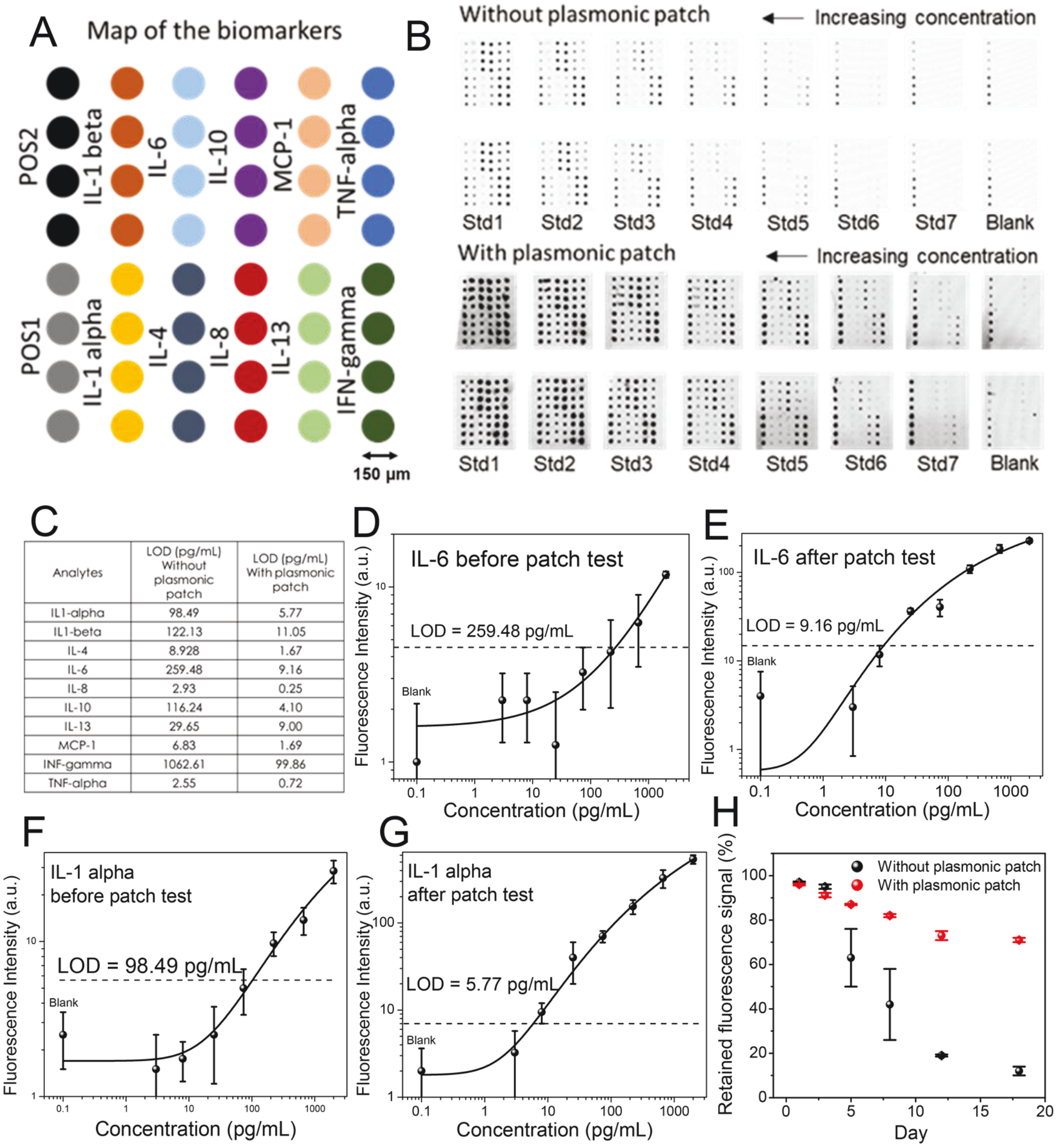

Analytes	LOD (pg/mL) Without plasmonic patch	LOD (pg/mL) With plasmonic patch
IL1-alpha	98.49	5.77
IL1-beta	122.13	11.05
IL-4	8.928	1.67
IL-6	259.48	9.16
IL-8	2.93	0.25
IL-10	116.24	4.10
IL-13	29.65	9.00
MCP-1	6.83	1.69
INF-gamma	1062.61	99.86
TNF-alpha	2.55	0.72

Figure 5. Quantitative measurement of a multiplexed microarray of 10 human cytokines using a AuNR size-optimized plasmonic patch. (A) Layout of the antibodies corresponding to the cytokines on the quantitative microarray. Each type of antibody is printed in quadruplicate on the glass substrate. (B) Fluorescence map of the 10-plex microarray under various analyte concentrations (standard 7 (Std7) to standard 1 (Std 1)). Top: without adding a plasmonic patch. Bottom: with plasmonic-patch enhancement. (C) Limit of detection of each cytokine before and after addition of the plasmonic patch. Standard curves of IL-6 (D) before and (E) after applying the plasmonic patch. Standard curves of IL-1 alpha (F) before and (G) after applying the plasmonic patch. (H) Comparison of the stability of fluorescence signals before and after addition of the plasmonic patch.

factor was found to increase with an increase in the density of the AuNRs on the plasmonic patch and essentially plateaued for densities higher than ~48/μm^2 (Figure 3C,D). Increasing the density of the large AuNRs (130 × 40 nm^2) beyond 60/μm^2 was found to be difficult. Similar saturation of the fluorescence enhancement factor was also observed for smaller AuNRs (57 × 18 nm^2) with the increase of the AuNR density on the patch (Figure S5).

To understand the saturation of the fluorescence enhancement factor with increasing AuNR density, we have employed FDTD simulations (Figure 3E−H). It is known that metal nanostructures at the LSPR wavelength can absorb and scatter significantly more light than directly incident on them.[26,27] The local time-averaged Poynting vector field around the AuNR at the longitudinal LSPR wavelength, which represents the optical power flow, was deduced using FDTD simulations (Figure 3F−H). Based on the calculated extinction spectrum, the extinction cross-section of a single AuNR (with a length of 130 nm and a diameter of 40 nm) at the longitudinal LSPR wavelength was determined to be 55,510 nm^2, which indicates that ~18 AuNRs/μm^2 are sufficient to absorb and confine most of the incident light.[28] In the FDTD simulation, the electric field of the incident plane wave was set to be parallel to the long-axis of the AuNR (Figure 3F). However, since the AuNRs on the plasmonic patch are randomly orientated with respect to the polarization of the incident beam, the experimentally determined density of AuNRs (40−50 AuNRs/μm^2) for saturation of the fluorescence enhancement factor was slightly higher than that estimated from the FDTD calculations (18 AuNRs/μm^2).

https://dx.doi.org/10.1021/acsami.0c20303
ACS Appl. Mater. Interfaces 2021, 13, 11414−11423

Following the optimization of the AuNR size effect as well as its density on the plasmonic patch, we set out to test the applicability (aspect ratio ~3.25, AuNR-130 × 40 nm^2, density ~55.6 ± 2.7/μm^2) in improving the bioanalytical parameters (i.e., sensitivity, limit of detection, dynamic range) of a conventional fluoroimmunoassay. Human interlukin-6 (IL-6) was employed as the target protein biomarker, which acts as both an anti-inflammatory and proinflammatory cytokine.[29] Recent studies suggested that salivary and serum IL-6 (together with other cytokines) hold promise as biomarkers for oral squamous cell carcinoma (OSCC).[30−32] In contrast to other cancer biomarkers, such as prostate-specific antigen (PSA), the concentrations of IL-6 concentration in serum (both healthy and diseased state) are around 1000-fold lower.[33] The IL-6 level in healthy human serum ranges from a few fg/mL to about 6 pg/mL.[34] Under pathological conditions, it can be present at higher concentrations.

Here, we postulated that a plasmonic patch with optimal AuNR dimensions as a fluorescence signal enhancer in an IL-6 fluoroimmunoassay would significantly improve the bioanalytical parameters (e.g., sensitivity and dynamic range) due to the large fluorescence enhancement offered by the AuNR size-optimized plasmonic patch. In accordance with the standard workflow of ELISA, a 96-well plate was used to perform this assay, which involves (i) immobilization of the IL-6 capture antibody, (ii) capture of the IL-6 by the immobilized antibody, (iii) binding of the biotinylated detection antibody to the captured IL-6, and (iv) binding of a fluorophore (800CW)-labeled streptavidin to the biotinylated detection antibody. Finally, a plasmonic patch was simply added onto the top of the immunosandwich as the new, last step (Figure 4A).

To investigate the improvement in sensitivity and dynamic range of the fluoroimmunoassay, IL-6 with known concentrations (0.006−6000 pg/mL in 1% BSA) as well as blank control were employed as standards. The fluorescence images obtained before applying the plasmonic patch showed an extremely weak signal with a limit of detection (LOD) of ~600 pg/mL (Figure 4B). The fluorescence intensity was significantly enhanced after applying plasmonic patches comprised of AuNR-57 × 18 nm^2 and AuNR-130 × 40 nm^2 (Figure 4C,D and Figure S6). Notably, the LOD (3σ) of the plasmon-enhanced IL-6 assay was calculated to be 0.2 pg/mL (five-parameter logistic (5PL) fit) using a plasmonic patch comprised of AuNR-130 × 30 nm^2, which is ~30 times lower compared to the LOD obtained using the suboptimal plasmonic patch comprised of AuNR-57 × 18 nm^2 (~5.8 pg/mL, 5PL fit). In addition to the enhanced sensitivity, the plasmonic-patch-enhanced fluoroimmunoassay showed a significantly larger dynamic range (from 0.2 pg/mL to 6 ng/mL) compared to that of vendor-specified ELISA (R&D systems, DY206). These results further validate the importance of optimizing the plasmonic nanostructures, and by extension the plasmonic patch, for various bioanalytical applications.

Finally, we applied the plasmonic patch comprised of AuNRs with optimal dimensions on a quantitative protein microarray to test the feasibility of using a plasmonic patch to simultaneously enhance the limit of detection of multiple protein biomarkers. Here, human inflammation microarrays for 10 cytokines were employed and the capture antibody for each cytokine together with the positive controls are arrayed in quadruplicate on the glass slide with a feature diameter of 150 μm (Figure 5A). To determine the limit of detection for each cytokine in the microarray, the array specific cytokine standards, whose concentration has been predetermined, were employed. Next, a biotin-labeled detection antibody cocktail was added to recognize a different epitope of the cytokine, followed by the addition of the streptavidin-800CW fluorophore. Finally, a plasmonic patch (with large AuNR-130 × 40 nm^2) was applied on the microarray. The fluorescence map of the microarray revealed a large enhancement in the fluorescence signal for all of the target analytes at different concentrations after the addition of a plasmonic patch on the microarray (Figure 5B). The size and shape of the fluorescent microspots remain mostly unaltered, reflecting the uniform distribution of AuNRs on the plasmonic patch down to micro scale (Figure S7). We noted a significant improvement in the limit of detection for all 10 of the cytokines (Figure 5C and Figure S8). Notably, the limit of detection of IL-6 was lowered from 259.48 to 9.16 pg/mL, indicating a 28-fold improvement in the sensitivity (Figure 5D,E). In addition to the improved sensitivity for each cytokine, the coefficient of variation (CV) of the fluorescent signal after the plasmonic patch was added was smaller compared to the nonenhanced fluorescence microarray (Figure 5D−G and Figure S8). This can be attributed to the significantly enhanced fluorescence signal, which is much higher than the interference noise level from the background as well as the fluorescence detector.

In addition to the large fluorescence enhancement, we note that the fluorescent surface (e.g., surface coated with 800CW fluorophores) covered with a plasmonic patch retained nearly 70% signal after 2 weeks of storage under ambient conditions, as opposed to nearly 90% loss in signal intensity of an uncovered surface stored under identical conditions. This can be attributed to the close contact between the fluorophore and the PDMS film, which protects the fluorophores from being oxidized and therefore slows down the dye degradation process. The high signal stability using a plasmonic patch opens the possibility of shipping the bioassay samples to centralized clinical laboratories for analysis or for archiving.

SEM images of 16 different plasmonic patches showed a uniform distribution of AuNRs, with a small relative standard deviation (~5%) in the AuNR density across different patches (Figure S9). Due to the flexibility, conformability, and uniformity of the plasmonic patch, we expect this technology to be broadly applicable across diverse fluorescence-based bioanalytical methods such as fluoroimmunoassays, immunomicroarrays, fluoroSPOT, and in vitro imaging.

■ CONCLUSIONS

To summarize, we have systematically studied the effect of the size of the AuNRs on their fluorescence enhancement efficiency. We found that, in addition to the LSPR wavelength of the plasmonic nanostructures, their absolute dimensions are critical for maximizing the fluorescence enhancement obtained using a plasmonic patch. The optimal dimensions of the AuNRs determined using FDTD simulations for attaining maximum electromagnetic field enhancement showed excellent agreement with experimentally determined dimensions of the AuNRs that exhibited the highest fluorescence enhancement. Compared to the unenhanced fluoroimmunoassay, the AuNR size-optimized plasmonic-patch-enhanced fluoroimmunoassay exhibited 3 orders of magnitude lower limit of detection. High sensitivity and large dynamic range combined with the use of established bioassay platforms (e.g., 96-well plates, multiplex microarrays, standard affinity reagents, read-out devices) and work-flow make the plasmon-enhanced fluoroimmunoassays highly attractive for research and clinical applications.

■ EXPERIMENTAL SECTION

Materials. Polydimethylsiloxane (PDMS), cetyltrimethylammonium bromide (CTAB), ascorbic acid, chloroauric acid, sodium borohydride, tris(hydroxymethyl)amino methane (tris), poly(stryrene sulfonate) (PSS) (Mw = 100,000 g/mol), (3-aminopropyl)-trimethoxysilane (APTMS), and trimethoxypropylsilane (TMPS) were purchased from Sigma-Aldrich (St. Louis, MO). Silver nitrate was purchased from VWR International. The IL-6 ELISA kit (DY 206) was purchased from R&D systems (Minneapolis, MN). Concentrated phosphate buffered saline (PBS) was purchased from Omnipur. All chemicals have been used as received with no further purification.

Synthesis of Gold Nanorods (AuNRs). AuNRs were synthesized using a seed-mediated approach.[35] Seed solution was prepared by adding 0.6 mL of an ice-cold sodium borohydride solution (10 mM) into 10 mL of CTAB (0.1 M) and chloroauric acid (2.5×10^{-4} M) solution under vigorous stirring at 25 °C. The color of the seed solution changed from yellow to brown. For synthesizing AuNRs with different wavelengths, growth solutions were prepared by mixing 38 mL of CTAB (0.1 M), 0.25 mL (or 0.3, 0.35, 0.4, 0.45, 0.5, 0.55, and 0.6 mL for different LSPR wavelengths) of silver nitrate (10 mM), 2.0 mL of chloroauric acid (10 mM), and 0.22 mL of ascorbic acid (0.1 M) in that order. Then, 48 μL of freshly prepared seed solution was added into the growth solution and this solution was kept in the dark overnight to obtain AuNRs with different LSPR wavelengths.

For synthesizing AuNRs with different sizes, growth solution was prepared by mixing 38 mL of CTAB (0.1 M), 0.25 mL (or 0.30, 0.35, 0.40, 0.45, 0.50, 0.55, and 0.6 mL for different sizes) of silver nitrate (10 mM), 2.0 mL of chloroauric acid (10 mM), 0.22 mL of ascorbic acid (0.1 M), and 0.8 mL of HCl (1.0 M) consecutively. Subsequently, 0.2 μL (or 0.4, 2.5, 5, 10, 25, 30, and 48 μL for different sizes) of freshly prepared seed solution was added into the growth solution and this solution was kept in the dark overnight to obtain AuNRs with different sizes. Finally, the AuNR was washed by centrifugation and redispersed in nanopure water to achieve a final extinction of 2.0.

Plasmonic Patch Preparation. Sylgard 186 (Dow Corning) polydimethylsiloxane prepolymer was mixed with curing agent at a 10:1 (polymer to curing agent) ratio. This mixture was spin coated at a speed of 3000 rpm for 30 s on a 35 mm diameter polystyrene Petri dish. The PDMS film was then cured at 60 °C for 12 h. In order to facilitate the adsorption of AuNRs on PDMS, the PDMS film was first treated by oxygen plasma for 3 min, followed by treatment with 2 mL of 0.2% aqueous poly(styrenesulfonate) (PSS) for 20 min (this step facilitates the adsorption of AuNR on PDMS film through electrostatic interactions between positively charged AuNR and negatively charged PSS). Then, 1 mL of AuNR solution (described above) was centrifuged and redispersed into 1.5 mL of nanopure water. For synthesizing the plasmonic patch AuNR-130 × 40 nm^2 with decreasing density of AuNRs, 2.0, 1.5, 1.0, 0.5, 0.25, and 0.125 mL of AuNR solution was centrifuged and redispersed into 1.5 mL of nanopure water. Subsequently, the PSS-treated PDMS film was incubated with the above-mentioned 1.5 mL AuNR solution for 15 h in the dark. Finally, the PDMS films were rinsed with nanopure water to remove weakly bound AuNRs and blow-dried under a stream of nitrogen. AuNRs were uniformed distributed on the PDMS film with a random orientation.

Polymer Spacer on Plasmonic Patch. In order to optimize the distance between the AuNR surface and fluorophores, a thin layer of polysiloxane was formed on the surface of the AuNR. For this purpose, 8 μL of APTMS and 0.25 μL of TMPS were added into 3 mL of phosphate buffered saline (1× PBS). Then, the plasmonic patch was incubated in this solution for 2 h at room temperature. After 2 h, the plasmonic patch was rinsed with PBS and nanopure water and blow-dried under a steam of nitrogen.

Fluorescence Measurement. The optical data was collected using an LI-COR Odyssey CLx fluorescence scanner. A solid state diode laser was employed as the excitation source that simultaneously provides light at 785 nm. The light from the fluorescing species in the sample (as well as other light generating sources) was subsequently passed to a dichroic mirror, which splits the light and essentially sorts the fluorescent signals by transmitting the light above 810 nm and reflecting the light below 750 nm. Transmitted and reflected light travels two independent paths through optics designed to remove scattered and stray light. Polystyrene wells (standard 96-well plate) were uniformly coated with 800CW by incubation with 10 ng/mL 800CW-labeled streptavidin (in 1× PBS) for 30 min. The wells were subsequently washed three times each using 1× PBS and nanopure water. The plasmonic patch was cut into a circular shape with a diameter around 5 mm using a biopsy punch (Fisher Scientific, catalog number: 12-460-412), which was then transferred to the polystyrene surface using tweezers. Increasing the PDMS film thickness to 60 μm resulted in a slight increase (19%) in the fluorescence enhancement efficiency on planar surfaces (Figure S10). However, further increase in the PDMS thickness is expected to deteriorate the conformability of the plasmonic patch, leading to a decrease in the fluorescence enhancement efficiency, especially when applied on nonplanar surfaces or microstructured surfaces such as cells and tissues.

Plasmonic-Patch-Enhanced Fluoroimmunoassay. Plasmonic-patch-enhanced fluoroimmunoassay was implemented using 96-well plates with a plastic bottom. The plate was first incubated with IL-6 capture antibody (2 μg/mL in PBS) overnight followed with 1.5 h of blocking using 3% BSA. Portions of 100 μL of standard solutions with different IL-6 concentrations were then added into appropriate wells. The plate was sealed and then gently shaken for 2.5 h at room temperature. The solution was then discarded, and the wells were washed four times with washing buffer (1× PBS with 0.05% Tween 20). Subsequently, 100 μL of biotinylated antibody solution (50 ng/mL) was added into each well and incubated for 2 h at room temperature. After washing, 100 μL of 800CW-labeled streptavidin (50 ng/mL) was added to each well followed by 20 min of incubation. The plates were washed three times each with washing buffer followed by nanopure water. Finally, the plasmonic patch was transferred onto each well of the 96-well plate, followed by the addition of a reflective layer on the top. Uniform application of the plasmonic patch was achieved with the help of residual water on the microtiter well surface after the last washing step. The final step in a fluoroimmunoassay involves extensive washing, which leaves a thin layer of water at the bottom of the microwell. Plasmonic patch film can spread on the surface due to capillary force, which ultimately holds the film uniformly and firmly on the fluorescent tags bound to the detection antibody. The plate was incubated at 40 °C for 20 min to allow the evaporation of any liquid. A LICOR Odyssey CLx scanner was used to scan the 96-well plate.

Plasmonic-Patch-Enhanced Fluorescence Microarray. A commercialized protein quantitative microarray kit was purchased from RayBiotech (Quantibody Human Inflammation Array 1, QAH-INF-1). Antibodies were printed on a glass slide with 16 subarrays available per slide. The slide was blocked by blocking buffer (in kit) for 30 min. Standard samples with various cytokine concentrations and blank control sample were prepared and were added into each subwell of the microarray chip followed by a 2 h incubation at room temperature. The chip was then washed thoroughly with wash buffer (in kit). Next, 70 μL of biotin-conjugated anticytokine cocktail (in a kit) was added to each subarray and the chip was incubated at room temperature with gentle shaking. After 2 h, the chip was washed and 70 μL of streptavidin-800CW (100 ng mL^{-1} in blocking buffer) and the plate was incubated under dark conditions for 20 min. The chip was washed thoroughly with wash buffer and then nanopure water and blow-dried under nitrogen gas. The glass chip was scanned by an Azure Sapphire imager using a 800 nm channel. Finally, a plasmonic patch of AuNR-760 was cut into 1 × 1 cm^2 and applied on the top of each subarray. The chip was rescanned using the same settings.

■ ASSOCIATED CONTENT

Supporting Information

The Supporting Information is available free of charge at https://pubs.acs.org/doi/10.1021/acsami.0c20303.

> Figure S1, fluorescence enhancement efficiency dependence on AuNR LSPR wavelength; Figure S2, AuNR fluorescence enhancement efficiency under different electromagnetic field intensity enhancements; Figure S3, autofluorescence of the plasmonic patch; Figure S4, extinction spectra of AuNR (130×40 nm^2) colloidal solutions of varying concentrations; Figure S5, fluorescence enhancement efficiency dependence on LSPR wavelength for AuNR with a size around 57×18nm^2; Figure S6, IL-6 dose−response curve of AuNR (57×18 nm^2) enhanced and AuNR (130×40 nm^2) enhanced fluoroimmunoassay; Figure S7, high resolution fluorescence map of the 10-plex microarray; Figure S8, standard curves of IL-1 alpha, IL-1 beta, IL-4, IL-6, IL-8, IL-10, IL-13, MCP-1, IFNgamma, and TNF-alpha before and after applying the plasmonic patch; Figure S9, SEM characterizations of the AuNR distribution on 16 different plasmonic patches; Figure S10, fluorescence enhancement efficiency of plasmonic patches with different thicknesses (PDF)

■ AUTHOR INFORMATION

Corresponding Authors

Rajesh R. Naik − *711th Human Performance Wing, Air Force Research Laboratory, Wright-Patterson Air Force Base, Dayton, Ohio 45433, United States;* orcid.org/0000-0002-7677-928X; Email: rajesh.naik@us.af.mil

Srikanth Singamaneni − *Department of Mechanical Engineering and Materials Science, Institute of Materials Science and Engineering and Siteman Cancer Center, Washington University in St. Louis, St Louis, Missouri 63130, United States;* orcid.org/0000-0002-7203-2613; Email: singamaneni@wustl.edu

Authors

Chao Liang − *Department of Anesthesiology, Zhongshan Hospital, Fudan University, Shanghai 200032, China; Department of Mechanical Engineering and Materials Science, Institute of Materials Science and Engineering, Washington University in St. Louis, St Louis, Missouri 63130, United States*

Jingyi Luan − *Department of Mechanical Engineering and Materials Science, Institute of Materials Science and Engineering, Washington University in St. Louis, St Louis, Missouri 63130, United States*

Zheyu Wang − *Department of Mechanical Engineering and Materials Science, Institute of Materials Science and Engineering, Washington University in St. Louis, St Louis, Missouri 63130, United States*

Qisheng Jiang − *Auragent Bioscience LLC, St Louis, Missouri 63108, United States*

Rohit Gupta − *Department of Mechanical Engineering and Materials Science, Institute of Materials Science and Engineering, Washington University in St. Louis, St Louis, Missouri 63130, United States*

Sisi Cao − *Department of Mechanical Engineering and Materials Science, Institute of Materials Science and Engineering, Washington University in St. Louis, St Louis, Missouri 63130, United States*

Keng-Ku Liu − *Auragent Bioscience LLC, St Louis, Missouri 63108, United States*

Jeremiah J. Morrissey − *Department of Anesthesiology and Siteman Cancer Center, Washington University in St. Louis, St. Louis, Missouri 63110, United States;* orcid.org/0000-0002-9911-4811

Evan D. Kharasch − *Department of Anesthesiology, Duke University School of Medicine, Durham, North Carolina 27710, United States;* orcid.org/0000-0002-6613-922X

Complete contact information is available at: https://pubs.acs.org/10.1021/acsami.0c20303

Author Contributions

○C.L., J.L.: These authors contributed equally to this work.

Notes

The authors declare the following competing financial interest(s): J.L., J.J.M., E.D.K., and S.S. are inventors on a provisional patent related to this technology, and the technology has been licensed by the Office of Technology Management at Washington University in St. Louis to Auragent Bioscience LLC. J.L., J.J.M., E.D.K., and S.S. are cofounders/shareholders of Auragent Bioscience LLC. These potential conflicts of interest have been disclosed and are being managed by Washington University in St. Louis.

■ ACKNOWLEDGMENTS

We acknowledge support from National Science Foundation (CBET-1900277, ECCS- 1908167) and National Institutes of Health (R01 CA141521). The authors thank Dr. Kristen Naegle for providing access to the LICOR Odyssey CLx scanner and Nano Research Facility (NRF) and Institute of Materials Science and Engineering (IMSE) at Washington University for providing access to electron microscopy facilities.

■ REFERENCES

(1) Anger, P.; Bharadwaj, P.; Novotny, L. Enhancement and quenching of single-molecule fluorescence. *Phys. Rev. Lett.* **2006**, *96* (11), 113002.

(2) Tam, F.; Goodrich, G. P.; Johnson, B. R.; Halas, N. J. Plasmonic enhancement of molecular fluorescence. *Nano Lett.* **2007**, *7* (2), 496−501.

(3) Trotsiuk, L.; Muravitskaya, A.; Kulakovich, O.; Guzatov, D.; Ramanenka, A.; Kelestemur, Y.; Demir, H. V.; Gaponenko, S. Plasmon-enhanced fluorescence in gold nanorod-quantum dot coupled systems. *Nanotechnology* **2020**, *31* (10), 105201.

(4) Flauraud, V.; Regmi, R.; Winkler, P. M.; Alexander, D. T.; Rigneault, H.; Van Hulst, N. F.; García-Parajo, M. F.; Wenger, J. r. m.; Brugger, J. r. In-plane plasmonic antenna arrays with surface nanogaps for giant fluorescence enhancement. *Nano Lett.* **2017**, *17* (3), 1703−1710.

(5) Tam, F.; Goodrich, G. P.; Johnson, B. R.; Halas, N. J. Plasmonic enhancement of molecular fluorescence. *Nano Lett.* **2007**, *7* (2), 496−501.

(6) Kinkhabwala, A.; Yu, Z.; Fan, S.; Avlasevich, Y.; Müllen, K.; Moerner, W. Large single-molecule fluorescence enhancements produced by a bowtie nanoantenna. *Nat. Photonics* **2009**, *3* (11), 654−657.

(7) Tabakman, S. M.; Lau, L.; Robinson, J. T.; Price, J.; Sherlock, S. P.; Wang, H.; Zhang, B.; Chen, Z.; Tangsombatvisit, S.; Jarrell, J. A. Plasmonic substrates for multiplexed protein microarrays with

femtomolar sensitivity and broad dynamic range. *Nat. Commun.* **2011**, *2*, 466.

(8) Zhang, B.; Kumar, R. B.; Dai, H.; Feldman, B. J. A plasmonic chip for biomarker discovery and diagnosis of type 1 diabetes. *Nat. Med.* **2014**, *20* (8), 948−953.

(9) Zhang, B.; Pinsky, B. A.; Ananta, J. S.; Zhao, S.; Arulkumar, S.; Wan, H.; Sahoo, M. K.; Abeynayake, J.; Waggoner, J. J.; Hopes, C. Diagnosis of Zika virus infection on a nanotechnology platform. *Nat. Med.* **2017**, *23* (5), 548−550.

(10) Liu, B.; Li, Y.; Wan, H.; Wang, L.; Xu, W.; Zhu, S.; Liang, Y.; Zhang, B.; Lou, J.; Dai, H. High Performance, Multiplexed Lung Cancer Biomarker Detection on a Plasmonic Gold Chip. *Adv. Funct. Mater.* **2016**, *26* (44), 7994−8002.

(11) Mayer, K. M.; Hafner, J. H. Localized surface plasmon resonance sensors. *Chem. Rev.* **2011**, *111* (6), 3828−3857.

(12) Haes, A. J.; Chang, L.; Klein, W. L.; Van Duyne, R. P. Detection of a biomarker for Alzheimer's disease from synthetic and clinical samples using a nanoscale optical biosensor. *J. Am. Chem. Soc.* **2005**, *127* (7), 2264−2271.

(13) Bardhan, R.; Grady, N. K.; Cole, J. R.; Joshi, A.; Halas, N. J. Fluorescence enhancement by Au nanostructures: nanoshells and nanorods. *ACS Nano* **2009**, *3* (3), 744−752.

(14) Guzatov, D. V.; Vaschenko, S. V.; Stankevich, V. V.; Lunevich, A. Y.; Glukhov, Y. F.; Gaponenko, S. V. Plasmonic enhancement of molecular fluorescence near silver nanoparticles: theory, modeling, and experiment. *J. Phys. Chem. C* **2012**, *116* (19), 10723−10733.

(15) Rose, A.; Hoang, T. B.; McGuire, F.; Mock, J. J.; Ciracì, C.; Smith, D. R.; Mikkelsen, M. H. Control of radiative processes using tunable plasmonic nanopatch antennas. *Nano Lett.* **2014**, *14* (8), 4797−4802.

(16) Pompa, P.; Martiradonna, L.; Della Torre, A.; Della Sala, F.; Manna, L.; De Vittorio, M.; Calabi, F.; Cingolani, R.; Rinaldi, R. Metal-enhanced fluorescence of colloidal nanocrystals with nanoscale control. *Nat. Nanotechnol.* **2006**, *1* (2), 126−130.

(17) Zhou, L.; Ding, F.; Chen, H.; Ding, W.; Zhang, W.; Chou, S. Y. Enhancement of immunoassay's fluorescence and detection sensitivity using three-dimensional plasmonic nano-antenna-dots array. *Anal. Chem.* **2012**, *84* (10), 4489−4495.

(18) Kelly, K. L.; Coronado, E.; Zhao, L. L.; Schatz, G. C. *The optical properties of metal nanoparticles: the influence of size, shape, and dielectric environment*; ACS Publications: Washington, DC, 2003.

(19) Abadeer, N. S.; Brennan, M. R.; Wilson, W. L.; Murphy, C. J. Distance and plasmon wavelength dependent fluorescence of molecules bound to silica-coated gold nanorods. *ACS Nano* **2014**, *8* (8), 8392−8406.

(20) Luan, J.; Morrissey, J. J.; Wang, Z.; Derami, H. G.; Liu, K.-K.; Cao, S.; Jiang, Q.; Wang, C.; Kharasch, E. D.; Naik, R. R.; Singamaneni, S. Add-on plasmonic patch as a universal fluorescence enhancer. *Light: Sci. Appl.* **2018**, *7* (1), 29.

(21) Luan, J.; Morrissey, J. J.; Wang, Z.; Derami, H. G.; Liu, K.-K.; Cao, S.; Jiang, Q.; Wang, C.; Kharasch, E. D.; Naik, R. R. Add-on plasmonic patch as a universal fluorescence enhancer. *Light: Sci. Appl.* **2018**, *7* (1), 29.

(22) Khatua, S.; Paulo, P. M.; Yuan, H.; Gupta, A.; Zijlstra, P.; Orrit, M. Resonant plasmonic enhancement of single-molecule fluorescence by individual gold nanorods. *ACS Nano* **2014**, *8* (5), 4440−4449.

(23) Novo, C.; Gomez, D.; Perez-Juste, J.; Zhang, Z.; Petrova, H.; Reismann, M.; Mulvaney, P.; Hartland, G. V. Contributions from radiation damping and surface scattering to the linewidth of the longitudinal plasmon band of gold nanorods: a single particle study. *Phys. Chem. Chem. Phys.* **2006**, *8* (30), 3540−3546.

(24) Hu, M.; Novo, C.; Funston, A.; Wang, H.; Staleva, H.; Zou, S.; Mulvaney, P.; Xia, Y.; Hartland, G. V. Dark-field microscopy studies of single metal nanoparticles: understanding the factors that influence the linewidth of the localized surface plasmon resonance. *J. Mater. Chem.* **2008**, *18* (17), 1949−1960.

(25) Lin, K.-Q.; Yi, J.; Hu, S.; Liu, B.-J.; Liu, J.-Y.; Wang, X.; Ren, B. Size Effect on SERS of gold nanorods demonstrated via single nanoparticle spectroscopy. *J. Phys. Chem. C* **2016**, *120* (37), 20806−20813.

(26) Ni, W.; Kou, X.; Yang, Z.; Wang, J. Tailoring longitudinal surface plasmon wavelengths, scattering and absorption cross sections of gold nanorods. *ACS Nano* **2008**, *2* (4), 677−686.

(27) Park, K.; Biswas, S.; Kanel, S.; Nepal, D.; Vaia, R. A. Engineering the optical properties of gold nanorods: independent tuning of surface plasmon energy, extinction coefficient, and scattering cross section. *J. Phys. Chem. C* **2014**, *118* (11), 5918−5926.

(28) Jain, P. K.; Lee, K. S.; El-Sayed, I. H.; El-Sayed, M. A. Calculated absorption and scattering properties of gold nanoparticles of different size, shape, and composition: applications in biological imaging and biomedicine. *J. Phys. Chem. B* **2006**, *110* (14), 7238−7248.

(29) Wang, G.; Huang, H.; Zhang, G.; Zhang, X.; Fang, B.; Wang, L. Dual amplification strategy for the fabrication of highly sensitive interleukin-6 amperometric immunosensor based on poly-dopamine. *Langmuir* **2011**, *27* (3), 1224−31.

(30) Dineshkumar, T.; Ashwini, B. K.; Rameshkumar, A.; Rajashree, P.; Ramya, R.; Rajkumar, K. Salivary and serum interleukin-6 levels in oral premalignant disorders and squamous cell carcinoma: diagnostic value and clinicopathologic correlations. *Asian Pacific journal of cancer prevention: APJCP* **2016**, *17* (11), 4899.

(31) Sahibzada, H. A.; Khurshid, Z.; Khan, R. S.; Naseem, M.; Siddique, K. M.; Mali, M.; Zafar, M. S. Salivary IL-8, IL-6 and TNF-α as potential diagnostic biomarkers for oral cancer. *Diagnostics* **2017**, *7* (2), 21.

(32) St. John, M. A. R.; Li, Y.; Zhou, X.; Denny, P.; Ho, C.-M.; Montemagno, C.; Shi, W.; Qi, F.; Wu, B.; Sinha, U. Interleukin 6 and interleukin 8 as potential biomarkers for oral cavity and oropharyngeal squamous cell carcinoma. *Arch. Otolaryngol., Head Neck Surg.* **2004**, *130* (8), 929−935.

(33) Wang, G.; He, X.; Chen, L.; Zhu, Y.; Zhang, X. Ultrasensitive IL-6 electrochemical immunosensor based on Au nanoparticles-graphene-silica biointerface. *Colloids Surf., B* **2014**, *116*, 714−9.

(34) Hong, D. S.; Angelo, L. S.; Kurzrock, R. Interleukin-6 and its receptor in cancer: implications for translational therapeutics. *Cancer* **2007**, *110* (9), 1911−28.

(35) Orendorff, C. J.; Gearheart, L.; Jana, N. R.; Murphy, C. J. Aspect ratio dependence on surface enhanced Raman scattering using silver and gold nanorod substrates. *Phys. Chem. Chem. Phys.* **2006**, *8* (1), 165−70.